International Journal of Microwave and Wireless Technologies, 2012, 4(5), 529–535.
doi:10.1017/S1759078712000281

RESEARCH PAPER

Wideband and wide-angle flat Radomes using dielectric and ferrite layers

MOHAMMAD KHALAJ-AMIRHOSSEINI AND SAYED MOHAMMAD JAVAD RAZAVI

A new structure is proposed in this article, to operate as wideband and wide-angle flat Radome. In this structure several dielectric and ferrite layers are placed successively, one next to the other, to behave as a matched layer. First, the relationship between the permittivity and permeability of a required fictitious mixed material is obtained. Then the required permittivity and permeability of dielectric and ferrite layers are obtained at desired incidence angle. The performance of the proposed structure is investigated and validated using some theoretical and simulation examples.

Keywords: Radomes, Dielectric and ferrite layers

Received 3 September 2011; Revised 12 February 2012; first published online 12 April 2012

I. INTRODUCTION

Radomes are important components of antenna systems because they are sheltering structures to protect antennas against severe weather such as high winds, rain, icing, and/or temperature extremes [1]. On the other hand, Radomes must not interfere with normal operation of the antennas and so the input reflection of Radomes must be negligible at the usable frequency band of the protected antennas. So far, several structures have been introduced as Radomes such as single dielectric layer [2–6], multilayer dielectric slab [6–8], metal space frame [9–11], grooved dielectric layer [12], streamlined metallic [13], and inhomogeneous planar layer [14]. In this paper, we propose a new structure to operate as wideband and wide-angle flat Radome. In this structure several dielectric and ferrite layers are alternately located beside each other to behave as a single matched slow wave layer. First, the relationship between the permittivity and permeability of a required fictitious mixed material is obtained. Then the required permittivity and permeability of dielectric and ferrite layers are obtained at desired incidence angle. The performance of the proposed structure is investigated and validated using some theoretical and simulation examples.

II. RADOMES DESIGN

In this section, the idea to design wideband Radomes using dielectric and ferrite layers is presented. Figure 1(a) shows the cross section of a flat Radome of thickness d composed of a fictitious mixed material of permittivity ε_{rm} and of permeability μ_{rm}, called mixed material Radome (MMR). There have been quite a few patents based on this structure by composite materials [15, 16]. Also, Fig. 1(b) shows the cross section of a flat Radome of thickness d consisting of N cascaded basic structures, i.e. a ferrite (μ_r) layer between two dielectric (ε_r) layers. We call this Radome as dielectric ferrite Radome (DFR), which is consisting of $2N + 1$ successive dielectric and ferrite layers. It is proved in the next section that the performance of the DFRs can be an approximation of that of MMRs. The thickness Δz in Fig. 1(b) is given by

$$\Delta z = \frac{d}{2N}. \tag{1}$$

It is assumed that the incidence plane wave propagates in the free space obliquely with an angle of incidence θ_i. Also, two different polarizations are possible, one is the *TM* and the other is the *TE*. Of course, we know that the wave radiated by an antenna can be decomposed into many plane waves with different incidence angles. We would like to design the structures shown in Fig. 1 as Radomes in a wide incidence angle and at a wide frequency range. To analyze and design the proposed structures, the undesirable phenomena such as losses, frequency dispersion, and surface waves have not taken into account.

A) MMR design

The chain parameter matrix of the equivalent layer is given by [17]

$$\boldsymbol{T}_m = \begin{bmatrix} A_m & B_m \\ C_m & D_m \end{bmatrix} = \begin{bmatrix} \cos(k_m d) & jZ_m \sin(k_m d) \\ jZ_m^{-1} \sin(k_m d) & \cos(k_m d) \end{bmatrix}, \tag{2}$$

where k_m and Z_m are the propagation coefficient and the characteristic impedance of the MMR, respectively, given by

$$k_m = k_0 \sqrt{\mu_{rm}\varepsilon_{rm} - \sin^2(\theta_i)}, \tag{3}$$

College of Electrical Engineering, Iran University of Science and Technology, Narmak, Tehran, Iran
Corresponding author: M. Khalaj-Amirhosseini
Email: khalaja@iust.ac.ir

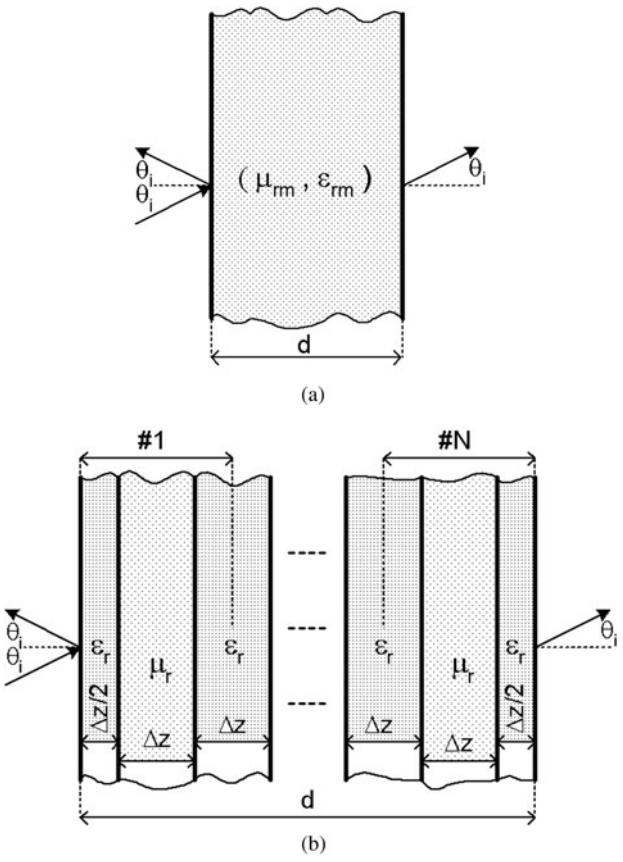

Fig. 1. (a) The cross section of a flat Radome of thickness d composed of a fictitious mixed material (MMR). (b) The cross section of a flat Radome of thickness d consisting of $2N+1$ dielectric and ferrite layers alternately (DFR).

$$Z_m = \begin{cases} \dfrac{\eta_o \mu_{rm}}{\sqrt{\mu_{rm}\varepsilon_{rm} - \sin^2(\theta_i)}}, & TE, \\ \dfrac{\eta_o}{\varepsilon_{rm}}\sqrt{\mu_{rm}\varepsilon_{rm} - \sin^2(\theta_i)}, & TM, \end{cases} \tag{4}$$

in which $k_o = 2\pi f/c$ (c is the velocity of the light) and η_o are the wave number and the impedance wave, respectively, in the free space. The reflection coefficients from two surfaces of the MMRs are given by [17]

$$\Gamma_{TE} = \frac{\mu_{rm}\cos(\theta_i) - \sqrt{\mu_{rm}\varepsilon_{rm} - \sin^2(\theta_i)}}{\mu_{rm}\cos(\theta_i) + \sqrt{\mu_{rm}\varepsilon_{rm} - \sin^2(\theta_i)}}, \tag{5}$$

$$\Gamma_{TM} = -\frac{\varepsilon_{rm}\cos(\theta_i) - \sqrt{\mu_{rm}\varepsilon_{rm} - \sin^2(\theta_i)}}{\varepsilon_{rm}\cos(\theta_i) + \sqrt{\mu_{rm}\varepsilon_{rm} - \sin^2(\theta_i)}}. \tag{6}$$

To have no reflection at desired incidence angle $\theta_i = \theta_o$ (similar to Brewster's angle), one of the following relations has to be held according to (5) and (6):

$$\begin{cases} \cos^2(\theta_o)\mu_{rm}^2 - \varepsilon_{rm}\mu_{rm} + \sin^2(\theta_o) = 0, & TE, \\ \cos^2(\theta_o)\varepsilon_{rm}^2 - \mu_{rm}\varepsilon_{rm} + \sin^2(\theta_o) = 0, & TM. \end{cases} \tag{7}$$

The relations in (7) translate the fact that the characteristic impedance of the MMR in (4) should be equal to that of free space, in order that the matching condition be satisfied. From (7), the relationship between the permittivity and permeability of the mixed material has to be as follows:

$$\begin{cases} \varepsilon_{rm} = \mu_{rm} - \dfrac{\mu_{rm}^2 - 1}{\mu_{rm}}\sin^2(\theta_o), & TE, \\ \mu_{rm} = \varepsilon_{rm} - \dfrac{\varepsilon_{rm}^2 - 1}{\varepsilon_{rm}}\sin^2(\theta_o), & TM. \end{cases} \tag{8}$$

It is seen that the required permittivity or permeability is dependent on the desired incidence angle. Here, we are looking for simultaneous validation of (8) for both *TE* and *TM* waves. In a special case of $\theta_o = 0^\circ$, which is the practical case for Radomes, the required permittivity and permeability must be equal to each other, i.e. $\varepsilon_{rm} = \mu_{rm}$, which gives a characteristic impedance equal to η_o at $\theta_i = 0^\circ$. In this case, the magnitude of *TE* and *TM* reflection coefficients becomes the same for all incidence angles as deduced from (5) and (6). Finally, substituting (8) in (5) and (6) yields us the following relations for the reflection coefficients of the surfaces, which are zero at $\theta_i = \theta_o$:

$$\Gamma_{TE} = \frac{1 - \sqrt{1 + \mu_{rm}^{-2}\dfrac{\sin^2(\theta_o) - \sin^2(\theta_i)}{\cos^2(\theta_o)}}}{1 + \sqrt{1 + \mu_{rm}^{-2}\dfrac{\sin^2(\theta_o) - \sin^2(\theta_i)}{\cos^2(\theta_o)}}}, \tag{9}$$

$$\Gamma_{TM} = -\frac{1 - \sqrt{1 + \varepsilon_{rm}^{-2}\dfrac{\sin^2(\theta_o) - \sin^2(\theta_i)}{\cos^2(\theta_o)}}}{1 + \sqrt{1 + \varepsilon_{rm}^{-2}\dfrac{\sin^2(\theta_o) - \sin^2(\theta_i)}{\cos^2(\theta_o)}}}. \tag{10}$$

B) DFR design

The construction of desired MMR materials is actually not practical. So, we approximate them by cascading N basic DFR structures as shown in Fig. 1(b). The chain parameter matrix of the whole DFR can be written as follows:

$$\boldsymbol{T} = \begin{bmatrix} A & B \\ C & D \end{bmatrix} = (\boldsymbol{T}_d\boldsymbol{T}_f\boldsymbol{T}_d)^N, \tag{11}$$

in which $\boldsymbol{T}_d$ and $\boldsymbol{T}_f$ are the chain parameter matrices of the dielectric and ferrite layers, respectively, as follows:

$$\boldsymbol{T}_d = \begin{bmatrix} \cos(k_d\Delta z/2) & jZ_d\sin(k_d\Delta z/2) \\ jZ_d^{-1}\sin(k_d\Delta z/2) & \cos(k_d\Delta z/2) \end{bmatrix}, \tag{12}$$

$$\boldsymbol{T}_f = \begin{bmatrix} \cos(k_f\Delta z) & jZ_f\sin(k_f\Delta z) \\ jZ_f^{-1}\sin(k_f\Delta z) & \cos(k_f\Delta z) \end{bmatrix}. \tag{13}$$

In (12) and (13), the propagation coefficients and the characteristic impedances are as follows:

$$k_d = k_o\sqrt{\varepsilon_r - \sin^2(\theta_i)}, \tag{14}$$

$$k_f = k_o\sqrt{\mu_r - \sin^2(\theta_i)}, \tag{15}$$

https://doi.org/10.1017/S1759078712000281 Published online by Cambridge University Press

$$Z_d = \begin{cases} \dfrac{\eta_o}{\sqrt{\varepsilon_r - \sin^2(\theta_i)}}, & TE, \\ \dfrac{\eta_o}{\varepsilon_r}\sqrt{\varepsilon_r - \sin^2(\theta_i)}, & TM, \end{cases} \tag{16}$$

$$Z_f = \begin{cases} \dfrac{\eta_o \mu_r}{\sqrt{\mu_r - \sin^2(\theta_i)}}, & TE, \\ \eta_o\sqrt{\mu_r - \sin^2(\theta_i)}, & TM. \end{cases} \tag{17}$$

The chain parameter matrices of dielectric and ferrite layers assuming $\Delta z \ll \lambda_o$, where λ_o is the wavelength in free space, can be approximated by

$$\boldsymbol{T}_d \cong \begin{cases} \begin{bmatrix} 1 & j\eta_o k_o \Delta z/2 \\ j\eta_o^{-1} k_o(\varepsilon_r - \sin^2(\theta_i))\Delta z/2 & 1 \end{bmatrix}, & TE, \\ \begin{bmatrix} 1 & j\eta_o \varepsilon_r^{-1}(\varepsilon_r - \sin^2(\theta_i))k_o \Delta z/2 \\ j\eta_o^{-1}\varepsilon_r k_o \Delta z/2 & 1 \end{bmatrix}, & TM, \end{cases} \tag{18}$$

$$\boldsymbol{T}_f \cong \begin{cases} \begin{bmatrix} 1 & j\eta_o \mu_r k_o \Delta z \\ j\eta_o^{-1}\mu_r^{-1}\left(\mu_r - \sin^2(\theta_i)\right)k_o \Delta z & 1 \end{bmatrix}, & TE, \\ \begin{bmatrix} 1 & j\eta_o\left(\mu_r - \sin^2(\theta_i)\right)k_o \Delta z \\ j\eta_o^{-1} k_o \Delta z & 1 \end{bmatrix}, & TM. \end{cases} \tag{19}$$

Therefore, the chain parameter matrix of a DFR with thickness $2\Delta z \ll \lambda_o$, can be approximated by

$$\begin{aligned} \boldsymbol{T}_{df} &= \boldsymbol{T}_d \boldsymbol{T}_f \boldsymbol{T}_d \\ &\cong \begin{cases} \begin{bmatrix} 1 & j\eta_o(\mu_r + 1)k_o \Delta z \\ j\eta_o^{-1}(\mu_r^{-1}(\mu_r - \sin^2(\theta_i)) & 1 \\ +(\varepsilon_r - \sin^2(\theta_i)))k_o \Delta z & \end{bmatrix}, & TE, \\ \begin{bmatrix} 1 & j\eta_o(\varepsilon_r^{-1}(\varepsilon_r - \sin^2(\theta_i)) \\ & +(\mu_r - \sin^2(\theta_i)))k_o \Delta z \\ j\eta_o^{-1}(\varepsilon_r + 1)k_o \Delta z & 1 \end{bmatrix}, & TM. \end{cases} \end{aligned} \tag{20}$$

On the other hand, the chain parameter matrix of the MMR (2) with thickness $2\Delta z \ll \lambda_o$, can be approximated by

$$\boldsymbol{T}_m \cong \begin{cases} \begin{bmatrix} 1 & j2\eta_o \mu_{rm} k_o \Delta z \\ j2\eta_o^{-1}\mu_{rm}^{-1} & 1 \\ \times(\mu_{rm}\varepsilon_{rm} - \sin^2(\theta_i))k_o \Delta z & \end{bmatrix}, & TE, \\ \begin{bmatrix} 1 & j2\eta_o \varepsilon_{rm}^{-1} \\ & \left(\mu_{rm}\varepsilon_{rm} - \sin^2(\theta_i)\right)k_o \Delta z \\ j2\eta_o^{-1}\varepsilon_{rm} k_o \Delta z & 1 \end{bmatrix}, & TM. \end{cases} \tag{21}$$

Comparing (20) with (21), the following relationships are obtained between the permittivity and permeability of MMRs and those of DFRs for *TE* and *TM* polarizations, respectively:

$$\begin{cases} \mu_{rm} = \dfrac{\mu_r + 1}{2}, \\ \varepsilon_{rm} = \dfrac{\varepsilon_r + 1}{2} - \dfrac{(\mu_r - 1)^2}{2\mu_r(\mu_r + 1)}\sin^2(\theta_i), \end{cases} \quad TE, \tag{22}$$

$$\begin{cases} \varepsilon_{rm} = \dfrac{\varepsilon_r + 1}{2}, \\ \mu_{rm} = \dfrac{\mu_r + 1}{2} - \dfrac{(\varepsilon_r - 1)^2}{2\varepsilon_r(\varepsilon_r + 1)}\sin^2(\theta_i), \end{cases} \quad TM. \tag{23}$$

It is seen that the equivalent permittivity or permeability varies with respect to the incidence angle, respectively, for *TE* and *TM* polarizations. At normal incidence, $\theta_i = 0$, the equivalent permittivity and permeability are the same for both *TE* and *TM* polarizations. Also, it is interesting to note that the equivalent permittivity and permeability are, respectively, the average of permittivities and permeabilities of the layers, at normal incidence, i.e. $\varepsilon_{rm} = (\varepsilon_r + 1)/2$ and $\mu_{rm} = (\mu_r + 1)/2$.

The above discussion leads us to design of DFRs. We choose either the permittivity or the permeability of the required mixed material and then use (8) to obtain the other one. Then, the required permittivity and permeability of dielectric and ferrite layers can be obtained from (22) or (23) at desired incidence angle. Of course, we have to actually choose the required permittivity and permeability of dielectric and ferrite layers equal to each other because θ_o is near to zero in Radomes.

Moreover, the chain parameter matrix of a DFR (11) can be used to find its reflection and transmission coefficients, as follows:

$$\Gamma = \frac{(A - Z_o C)Z_o + (B - Z_o D)}{(A + Z_o C)Z_o + (B + Z_o D)}, \tag{24}$$

$$T = \frac{2Z_o}{(A + Z_o C)Z_o + (B + Z_o D)}, \tag{25}$$

where Z_o is the transverse characteristic impedance of the free space given by

$$Z_o = \begin{cases} \dfrac{\eta_o}{\cos(\theta_i)}, & TE, \\ \eta_o \cos(\theta_i), & TM. \end{cases} \tag{26}$$

III. UNDESIRABLE PHENOMENA

In the proposed Radomes such as the conventional ones, there are some undesirable phenomena such as insertion phase delay, surface waves, losses, frequency dispersion and variation by temperature and power. In this section, two undesirable phenomena of insertion phase delay and surface waves are studied. It is assumed that $\varepsilon_{rm} = \mu_{rm} = (\varepsilon_r + 1)/2 = (\mu_r + 1)/2$ for MMRs and DFRs to keep $\theta_o = 0$ according to (8), (22), and (23).

A) Non-ideal ferrites

In the proposed structure the ferrite layers have been considered lossless and of permittivity equal to 1. However, in

https://doi.org/10.1017/S1759078712000281 Published online by Cambridge University Press

practice, the permittivity of ferrites may be greater than one along with they are lossy. In both cases, the discussion above the proposed structure could be still justifiable as shown below.

If the permittivity of ferrite layers is considered as $\varepsilon_{rf} \neq 1$, then one can obtain the following relations instead of (22) and (23):

$$\begin{cases} \mu_{rm} = \dfrac{\mu_r + 1}{2}, \\ \varepsilon_{rm} = \dfrac{\varepsilon_r + \varepsilon_{rf}}{2} - \dfrac{(\mu_r - 1)^2}{2\mu_r(\mu_r + 1)} \sin^2(\theta_i), \end{cases} \quad TE, \tag{27}$$

$$\begin{cases} \varepsilon_{rm} = \dfrac{\varepsilon_r + \varepsilon_{rf}}{2}, \\ \mu_{rm} = \dfrac{\mu_r + 1}{2} - \dfrac{(\varepsilon_r - \varepsilon_{rf})^2}{2\varepsilon_r\varepsilon_{rf}(\varepsilon_r + \varepsilon_{rf})} \sin^2(\theta_i), \end{cases} \quad TM. \tag{28}$$

Again, the equivalent permittivity and permeability are, respectively, the average of permittivities and permeabilities of the layers, at normal incidence.

Now, if the ferrite layers have an attenuation factor equal to $\alpha_f \neq 0$, their chain parameter matrices are modified from (13) to the following one:

$$\begin{aligned} \boldsymbol{T}_f &= \begin{bmatrix} \cosh\big((\alpha_f + jk_f)\Delta z\big) & Z_f \sinh\big((\alpha_f + jk_f)\Delta z\big) \\ Z_f^{-1} \sinh\big((\alpha_f + jk_f)\Delta z\big) & \cosh\big((\alpha_f + jk_f)\Delta z\big) \end{bmatrix} \\ &= \begin{bmatrix} \cos(k_f\Delta z) & jZ_f \sin(k_f\Delta z) \\ jZ_f^{-1} \sin(k_f\Delta z) & \cos(k_f\Delta z) \end{bmatrix} \\ &\quad \times \begin{bmatrix} \cosh(\alpha_f\Delta z) & Z_f \sinh(\alpha_f\Delta z) \\ Z_f^{-1} \sinh(\alpha_f\Delta z) & \cosh(\alpha_f\Delta z) \end{bmatrix}. \end{aligned} \tag{29}$$

It is seen that the chain matrix of a lossy ferrite layer is a multiplication of that of lossless ferrite layer by a matrix that indicates the insertion loss of the layer. So, the loss of ferrite and also dielectric layers can be extracted from the calculations and be considered as insertion loss.

B) Insertion phase delay

Ignoring Radome wall interface reflection effects, the insertion time delay (the difference between time delay of Radome and free space of the same thickness) can be expressed as follows for conventional dielectric Radomes, MMRs, and DFRs, respectively:

$$T_{DR} = \frac{d}{c}\left(\frac{\varepsilon_r}{\sqrt{\varepsilon_r - \sin^2(\theta_i)}} - \frac{1}{\cos(\theta_i)}\right), \tag{30}$$

$$T_{MMR} = \frac{d}{c}\left(\frac{\mu_{rm}\varepsilon_{rm}}{\sqrt{\mu_{rm}\varepsilon_{rm} - \sin^2(\theta_i)}} - \frac{1}{\cos(\theta_i)}\right), \tag{31}$$

$$\begin{aligned} T_{DFR} &\cong T_{MMR} \\ &= \frac{d}{c}\left(\frac{(\varepsilon_r + 1)^2}{2\sqrt{(\varepsilon_r + 1)^2 - 4\sin^2(\theta_i)}} - \frac{1}{\cos(\theta_i)}\right). \end{aligned} \tag{32}$$

As seen from (30) to (32), it results that $T_{MMR} \geq T_{DFR} > T_{DR}$ for the same thickness and permittivity.

C) Surface waves

From [17], the surface waves of a magneto-dielectric slab (MMR) have the following cut-off frequencies:

$$f_c = \frac{nc}{2d\sqrt{\varepsilon_{rm}^2 - 1}}, \tag{33}$$

where $n = 0, 1, 2, \ldots$ for TM_n and TE_n modes. Also, one can determine the phase constant (β) of dominant modes TM_0 and TE_0 along the surface of the Radomes from the following relationship:

$$\tan\left(k_0 \frac{d}{2}\sqrt{\varepsilon_{rm}^2 - (\beta/k_0)^2}\right) = \varepsilon_{rm}\sqrt{\frac{(\beta/k_0)^2 - 1}{\varepsilon_{rm}^2 - (\beta/k_0)^2}}. \tag{34}$$

After finding out β from (34), the attenuation factor of surface waves perpendicular to the Radome surface can be obtained as follows:

$$\alpha = \sqrt{\beta^2 - k_0^2}. \tag{35}$$

For DFRs, (33)–(35) can be approximately used through substituting $(\varepsilon_r + 1)/2$ for ε_{rm}.

IV. EXAMPLES AND RESULTS

In this section the operation of the proposed structure, DFR, as a wideband and wide-angle Radome is validated using some examples. Figures 2–4 illustrate the magnitude of *TE* and *TM* reflection coefficients of DFR and MMR at frequency $f = 10$ GHz versus μ_r and ε_r, d and θ_i, respectively, considering $N = 1, 2, 3$, and 4 cascaded basic structures. The assumptions of Figs 2–4 are ($d = 5$ mm and $\theta_i = \theta_0 = 0^\circ$), ($\mu_r = \varepsilon_r = 2$ and $\theta_i = \theta_0 = 0^\circ$), and ($\mu_r = \varepsilon_r = 2$, $\theta_0 = 0^\circ$ and $d = 5$ mm). The nulls appeared in Figs 2 and 3 are due to the fact that DFR acts almost as an MMR when its thickness is a half of the wavelength (inside DFR). Also, Figs 5 and 6 illustrate the magnitude of *TE* and *TM* reflection coefficients of DFR and MMR of thickness $d = 5$ mm at frequency $f = 10$ GHz versus θ_i assuming $\theta_0 = 45^\circ$ for *TE* and *TM* polarizations. Assuming $\theta_0 = 45^\circ$ for *TE* polarization requires $\mu_r = 2$, $\varepsilon_r = 1.25$, $\mu_{rm} = 1.5$, and $\varepsilon_{rm} = 1.083$ and that for *TM* polarization requires $\mu_r = 1.25$, $\varepsilon_r = 2$, $\mu_{rm} = 1.083$, and $\varepsilon_{rm} = 1.5$. From Figs 2–6 the accuracy of design relations (8), (22), and (23) is verified and it is seen that as the number of cascaded basic structures is increased the performances of DFRs approach those of MMRs which has no reflection at $\theta_i = \theta_0$.

Now, consider two DFRs of thickness $d = 5$ mm, $N = 4$, and $\mu_r = \varepsilon_r = 2$ and 1.2 ($\theta_0 = 0^\circ$) and also two simple homogeneous dielectric layers of thickness $d = 5$ mm (the same as for DFRs) and $\varepsilon_r = 2$ and 1.2. Figures 7 and 8 illustrate the magnitude of *TE* and *TM* reflection coefficients of two DFRs along with those of two dielectric layers versus incidence angle and the frequency as a parameter. Also, Figs 9 and 10 illustrate the magnitude of *TE* and *TM*

https://doi.org/10.1017/S1759078712000281 Published online by Cambridge University Press

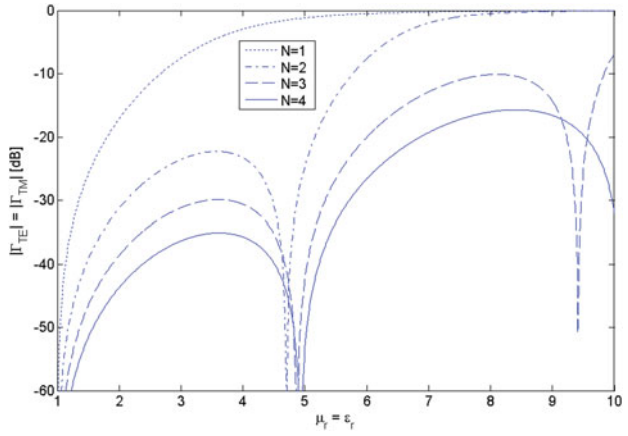

Fig. 2. The $|\Gamma_{TE}|$ and $|\Gamma_{TM}|$ of DFR at $f = 10$ GHz versus μ_r and ε_r, assuming $d = 5$ mm and $\theta_i = \theta_o = 0^\circ$ (those of MMR are minus infinite).

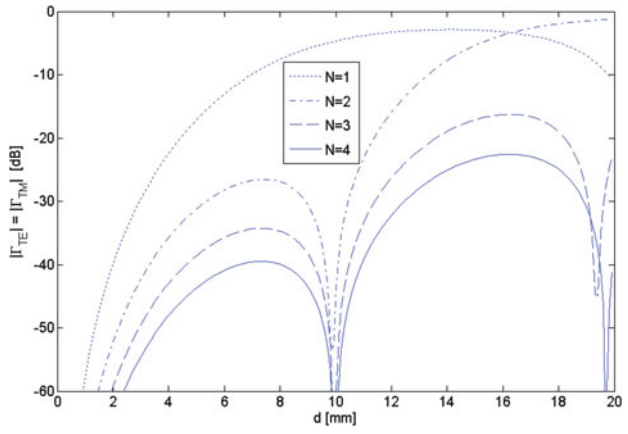

Fig. 3. The $|\Gamma_{TE}|$ and $|\Gamma_{TM}|$ of DFR at $f = 10$ GHz versus d, assuming $\mu_r = \varepsilon_r = 2$ and $\theta_i = \theta_o = 0^\circ$ (those of MMR are minus infinite).

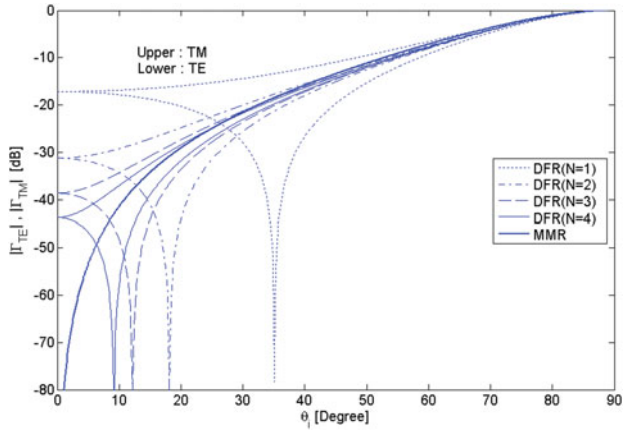

Fig. 4. The $|\Gamma_{TE}|$ and $|\Gamma_{TM}|$ of DFR and MMR at $f = 10$ GHz versus θ_i, assuming $d = 5$ mm and $\mu_r = \varepsilon_r = 2$ ($\theta_o = 0^\circ$).

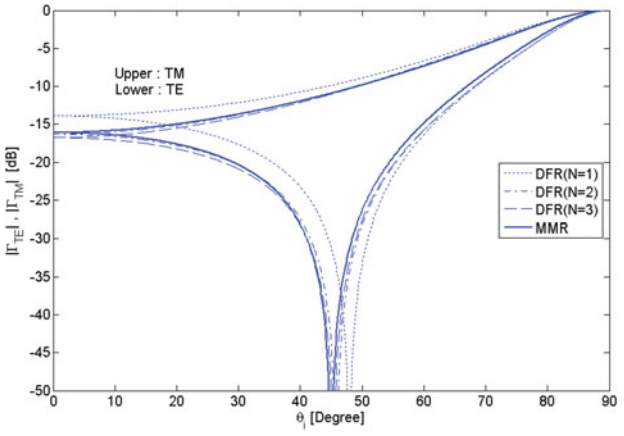

Fig. 5. The $|\Gamma_{TE}|$ and $|\Gamma_{TM}|$ of DFR and MMR at $f = 10$ GHz versus θ_i, assuming $d = 5$ mm, $\mu_r = 2$, $\varepsilon_r = 1.25$, $\mu_{rm} = 1.5$, and $\varepsilon_{rm} = 1.083$ ($\theta_o = 45^\circ$ for *TE*).

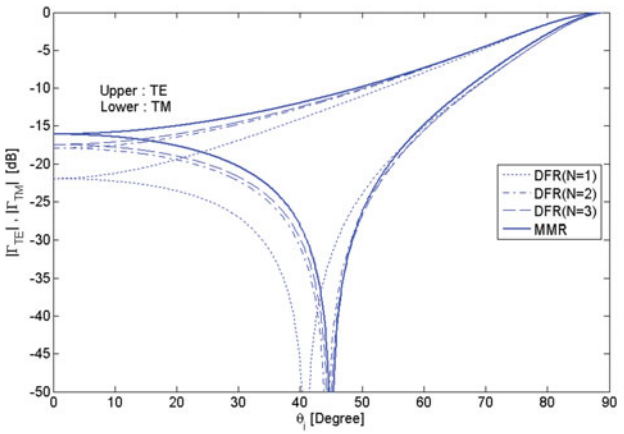

Fig. 6. The $|\Gamma_{TE}|$ and $|\Gamma_{TM}|$ of DFR and MMR at $f = 10$ GHz versus θ_i, assuming $d = 5$ mm, $\mu_r = 1.25$, $\varepsilon_r = 2$, $\mu_{rm} = 1.083$, and $\varepsilon_{rm} = 1.5$ ($\theta_o = 45^\circ$ for *TM*).

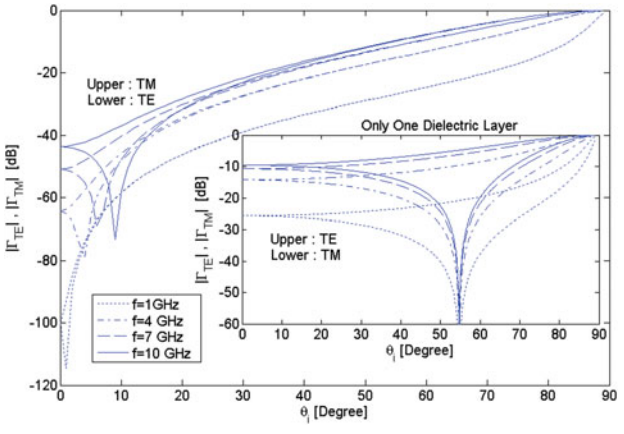

Fig. 7. The $|\Gamma_{TE}|$ and $|\Gamma_{TM}|$ of a DFR with $d = 5$ mm, $N = 4$ and $\mu_r = \varepsilon_r = 2$ ($\theta_o = 0^\circ$) and those of a homogeneous dielectric layer with $d = 5$ mm and $\varepsilon_r = 2$.

reflection coefficients of two DFRs versus frequency and the incidence angle as a parameter. It is seen from Figs 7–10 that the reflection coefficients of DFRs are much less than those of dielectric layers with the same permittivity and thickness. In other words, for a given value of the reflection coefficient, the allowed frequency and incidence angle ranges of DFRs are larger than those of dielectric layers. Therefore the potential superiority of DFRs with respect

https://doi.org/10.1017/S1759078712000281 Published online by Cambridge University Press

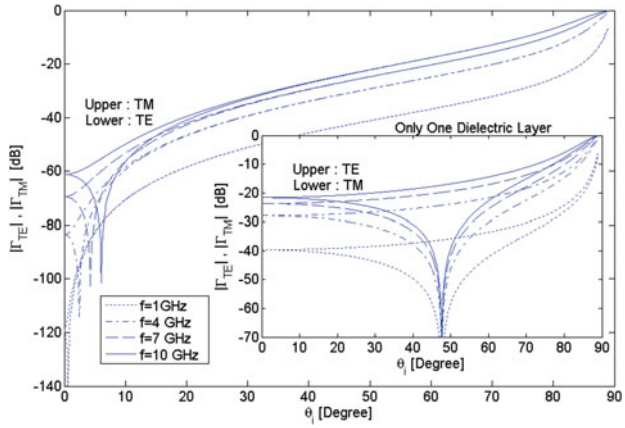

Fig. 8. The $|\Gamma_{TE}|$ and $|\Gamma_{TM}|$ of a DFR with $d = 5$ mm, $N = 4$, and $\mu_r = \varepsilon_r = 1.2$ ($\theta_o = 0^\circ$) and those of a homogeneous dielectric layer with $d = 5$ mm and $\varepsilon_r = 1.2$.

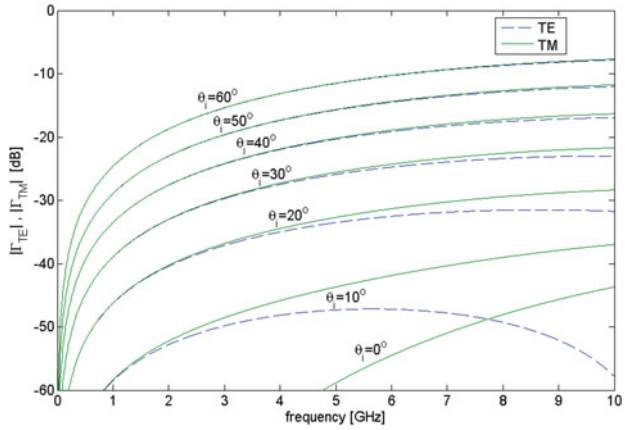

Fig. 9. The $|\Gamma_{TE}|$ and $|\Gamma_{TM}|$ of a DFR with $d = 5$ mm, $N = 4$, and $\mu_r = \varepsilon_r = 2$ ($\theta_o = 0^\circ$).

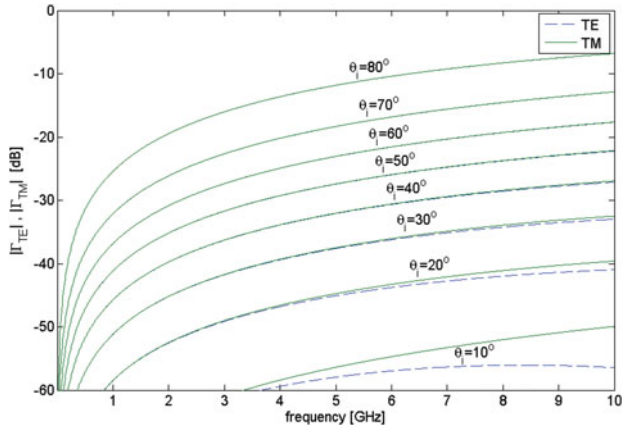

Fig. 10. The $|\Gamma_{TE}|$ and $|\Gamma_{TM}|$ of a DFR with $d = 5$ mm, $N = 4$, and $\mu_r = \varepsilon_r = 1.2$ ($\theta_o = 0^\circ$).

to dielectric layers for operating as wideband and wide-angle Radomes has now been proved. Also, it is seen that as the permittivity and permeability of DFRs and dielectric layer Radomes are chosen smaller, useful frequency band and incidence angle range are increased, which is an

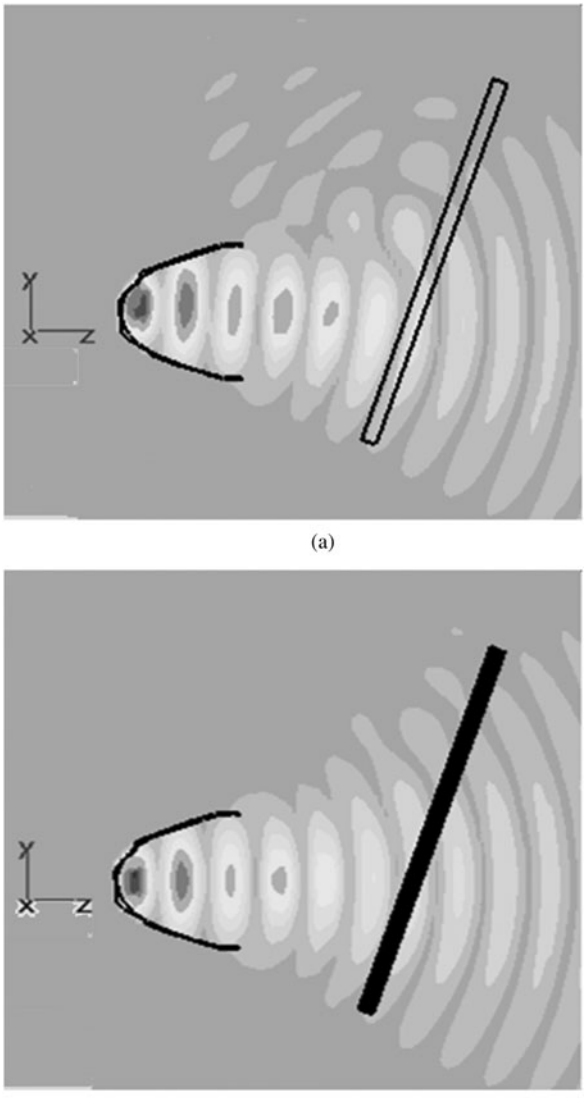

Fig. 11. The absolute of electric field for *TE* polarized incident wave at $f = 10$ GHz simulated by CST software. (a) a homogeneous dielectric layer with $d = 5$ mm and $\varepsilon_r = 2$. (b) a DFR with $d = 5$ mm, $N = 4$, and $\mu_r = \varepsilon_r = 2$ ($\theta_o = 0^\circ$).

evident fact. Therefore, to obtain better performance for DFRs, we should choose $\varepsilon_r = \mu_r$ and d as low as possible.

Finally, Fig. 11 demonstrates the propagation of *TE* polarized wave, at frequency 10 GHz and $\theta_i = 20^\circ$, created by a horn antenna with $\pm 20^\circ$ beam-width in front of a DFR ($d = 5$ mm, $N = 4$, and $\mu_r = \varepsilon_r = 2$) and a dielectric layer ($d = 5$ mm and $\varepsilon_r = 2$). This figure has been obtained from the full-wave simulator CST software. It is seen that the reflection of wave from DFR is much weaker than that of the dielectric layer Radome. In fact, Fig. 11 validates Fig. 7.

V. CONCLUSION

A new structure was proposed to operate as wideband and wide-angle flat Radome. In this structure several dielectric and ferrite layers are placed alternately beside each other to behave as a matched slow wave layer, while the permittivity and permeability of dielectric and ferrite layers are chosen

https://doi.org/10.1017/S1759078712000281 Published online by Cambridge University Press

equal to each other. The performance of the proposed structure was investigated and validated using some theoretical and simulation examples. It was observed that the reflection coefficients of DFRs are much less than those of dielectric layers with the same permittivity and thickness. Also, it was seen that as the permittivity of DFRs is decreased, useful frequency bandwidth and incidence angle range are increased.

REFERENCES

[1] Skolnik, M.I.: Introduction to RADAR systems, McGraw-Hill, New York, 1988.

[2] Chang, J.H.; Chan, K.K.: Analysis of a two-dimensional Radome of arbitrarily curved surface. IEEE Trans. Antennas Propag., **38** (10) (1990), 1565–1568.

[3] Zhao, W.J.; Li, L.W.; Gan, Y.B.: Efficient analysis of antenna radiation in the presence of airborne dielectric Radomes of arbitrary shape. IEEE Trans. Antennas Propag., **53** (1) (2005), 442–449.

[4] Wu, D.C.F.; Rudduck, R.C.: Plane wave spectrum-surface integration technique for Radome analysis. IEEE Trans. Antennas Propag., **22** (3) (1974), 497–500.

[5] Fathy, A.E.: Design of a near field protective dielectric Radome "Window" for a curved phased array antenna-circumferential polarization case. IEEE Trans. Antennas Propag., **54** (11) (2006), 3356–3366.

[6] Crone, G.A.E.; Rudge, A.W.; Mem, S.; Taylor, G.N.: Design and performance of airborne Radomes: a review. IEE Proc., **128** (7 Pt. F) (1981), 451–464.

[7] Dicaudo, V.J.: Determining optimum C-sandwich Radome thicknesses by means of smith chart. IEEE Trans. Antennas Propag., **15** (6) (1967), 821–822.

[8] Paris, D.T.: Computer-aided Radome analysis. IEEE Trans. Antennas Propag., **18** (1) (1970), 7–15.

[9] Kay, A.F.: Electrical design of metal space frame Radomes. IEEE Trans. Antennas Propag., **13** (2) (1965), 188–202.

[10] Meeks, M.L.; Ruze, J.: Evaluation of the Haystack antenna and Radome. IEEE Trans. Antennas Propag., **19** (6) (1971), 723–728.

[11] Altintas, A.; Ouardani, S.; Yurchenko, V.B.: Complex source radiation in a cylindrical Radome of metal-dielectric grating. IEEE Trans. Antennas Propag., **47** (8) (1999), 1293–1300.

[12] Bodnar, D.G.; Bassett, H.L.: Analysis of an anisotropic dielectric Radome. IEEE Trans. Antennas Propag., **23** (6) (1975), 841–846.

[13] Pelton, E.L.; Munk, B.A.: A streamlined metallic Radome. IEEE Trans. Antennas Propag., **22** (6) (1974), 799–803.

[14] Khalaj-Amirhosseini, M.: Wideband flat Radomes using inhomogeneous planar layers. Int. J. Antennas Propag., 2008 (Article ID 869720) (2008), 5.

[15] US Patent 7006052: Passive magnetic Radome. US Patent, February 28, 2006.

[16] USPTO P.A. 20070188397: Broadband polarized antenna including magnetodielectric material, isoimpedance loading, and associated methods.

[17] Balanis, C.A.: Advanced Engineering Electromagnetics, John Wiley & Sons, New York, USA, 1989.

Mohammad Khalaj-Amirhosseini was born in Tehran, in 1969. He received his B.Sc., M.Sc., and Ph.D. degrees from Iran University of Science and Technology (IUST) in 1992, 1994, and 1998, respectively, all in electrical engineering. He is currently an Associate Professor at College of Electrical Engineering of IUST. His scientific fields of interest are electromagnetic direct and inverse problems including microwaves, antennas, and electromagnetic compatibility.

Sayed Mohammad Javad Razavi was born in Kashan, Iran in 1976. He received the B.Sc. degree from Isfahan University of Technology (IUT), M.Sc. degree from Malek Ashtar University of Technology (MUT), Tehran, and Ph.D. degree from Iran University of Science and Technology (IUST) all in electrical engineering in 1999, 2002, and 2009, respectively. Currently, he is a researcher in EEUC/Electrical &Electronic University complex/MIUC Tehran, Iran.

https://doi.org/10.1017/S1759078712000281 Published online by Cambridge University Press